J. Fluid Mech. (1981), *vol.* 107, *pp.* 407–422
Printed in Great Britain

Gravitational convection from instantaneous sources on inclined boundaries

By P. BEGHIN, E. J. HOPFINGER
Institut de Mécanique (Laboratoire Associé au CNRS), Université de Grenoble, France
AND R. E. BRITTER
Engineering Department, University of Cambridge, Cambridge

(Received 29 April 1980)

Two-dimensional buoyant clouds moving along inclined boundaries under a gravitational force are investigated theoretically and experimentally. It is found that the 'thermal theory' gives a good description of the flow in the slope angle range $5° \lesssim \theta \leqslant 90°$. In this range the spatial growth rates of the cloud height and length are constant for a given slope angle and show a linear dependence on θ. For a cloud released with zero initial velocity the front velocity U_f first increases and then decreases, with the characteristic time of acceleration predicted by theory. In the decelerating state $U_f/(g_0' Q_0/x_f)^{\frac{1}{2}}$ is $2{\cdot}6 \pm 0{\cdot}2$ at $\theta \simeq 15°$, and then reduces uniformly with increasing θ to a value of $1{\cdot}5 \simeq 0{\cdot}2$ at 90° (where $g_0' Q_0$ is the released buoyancy and x_f is the front position measured from a virtual origin). The shape of the cloud is well approximated by a half-ellipse. The variation of the ratio of the principal axes of the half-ellipse with slope angle is identical with that of the head of an inclined starting plume (Britter & Linden 1980). However, the cloud has a greater growth rate than the head of a starting plume.

1. Introduction

The motion of an inclined turbulent buoyant cloud, referred to as inclined thermal, is relevant to a number of practical situations. The present work was in fact motivated by an attempt to understand powder snow avalanches better, but related phenomena of practical importance are leaks from liquified natural gas reservoirs, turbidity currents off the continental shelf and other fronts on slopes. In these flows the density difference giving rise to the buoyant force has different origins. There is, however, little difference between suspension flows and molecular weight or solute produced flows, provided the free fall velocity of the suspended particles is small compared with the turbulent velocity, so that their relative motion is negligible. In some cases the density difference may be quite large and the Boussinesq approximations violated, but the present work considers small density differences only.

The flow structure may be either that of a starting plume or a thermal, depending on whether the source is maintained or instantaneous. For an inclined starting plume the head has no effect on the development of the flow behind the head, but this flow, because of its higher velocity, feeds buoyancy into the head. This has the effect of keeping the front velocity a constant fraction of the plume velocity behind the head

and proportional to the cube root of the buoyancy flux at the source (Tochon-Danguy & Hopfinger 1975; Britter & Linden 1980).† In the case of a thermal the buoyancy is constant and the front velocity is a function of distance. It is of interest to study inclined thermals because, apart from their direct relevance to many applications, there are similarities between the thermal and the head of a starting plume (see, for example, Turner 1962). Also, when the source of a starting plume is removed a thermal will develop eventually.

In this paper two-dimensional inclined thermals are studied on inclines of slope angles ranging mainly from 5° to 90°. Some runs were also carried out with slope angles less than 5°. At zero slope the flow is equivalent in structure to a gravity current (Britter & Simpson 1978) and at 90° the two-dimensional line thermal studied by Tsang (1971) is approached. Because of the presence of the wall the flow consists in a half thermal with its mirror image behind the wall. The wall boundary layer is sufficiently small to be neglected and the shear stress on the wall has no effect on the dynamics except for angles well below 5°. In §4 the experimental results are presented for $5° \leqslant \theta \leqslant 90°$ and compared with the similarity theory developed in §2. The situation for $0 \leqslant \theta \leqslant 5°$ is discussed in §5.

2. The thermal theory

In the theoretical treatment the assumptions made for free vertical thermals (Morton, Taylor & Turner 1956) are adopted for inclined two-dimensional buoyant clouds. Furthermore, friction on the wall can be neglected for slope angles θ with respect to horizontal greater than a few degrees. Experiments show (see §4) that the thermal theory is applicable for $5° \lesssim \theta \leqslant 90°$, and gives a good description even for smaller angles (see §5).

The change in total linear momentum of the thermal, assuming that $\Delta\rho/\rho_a \ll 1$, is

$$\frac{d\rho_a(1+k_v)S_1HLU}{dt} = B\sin\theta, \tag{1}$$

where B is the total buoyancy $B = g(\rho-\rho_a)HLS_1$, which is invariant in uniform surroundings, S_1 is a shape factor, defined by S_1 = cross-sectional area/HL, ρ_a is the ambient fluid density, U the mass-centre velocity and H and L are respectively the height and length of the thermal. It is reasonable to take for the added mass coefficient k_v the value for an elliptic cylinder, which is $k_v = 2H/L$ (Batchelor 1974, p. 431).

The mass conservation equation reduces to

$$\frac{d}{dt}(S_1HL) = S_2(HL)^{\frac{1}{2}}\alpha(\theta)U, \tag{2}$$

where S_2 is another shape factor given by S_2 = circumference/$(HL)^{\frac{1}{2}}$. For a half-elliptic form which, as will be seen later, is a good representation of the observed flow, $S_1 = \frac{1}{4}\pi$ and $S_2 = (\pi/2^{\frac{3}{2}})(4k^2+1)^{\frac{1}{2}}/k^{\frac{1}{2}}$, with $k = H/L$. The entrainment co-

† Britter & Linden refer to the inclined starting plume as 'gravity current on inclines'. Both terminologies are possible and are in use.

efficient α is a function of slope angle only. The Reynolds number is assumed to be high, so that the thermal is turbulent.† Using $U = dx/dt$, equation (2) gives

$$H = \frac{1}{2}\frac{S_2}{S_1}k^{\frac{1}{2}}\alpha x, \tag{3}$$

$$L = \frac{1}{2}\frac{S_2}{S_1}k^{-\frac{1}{2}}\alpha x, \tag{4}$$

where x is here measured from the 'virtual origin' defined by $H = L = 0$.

When using (3) and (4) in (1) the equation for the mass-centre velocity has the form:

$$U\frac{d}{dx}(x^2U) = \frac{4}{(1+k_v)}\frac{S_1}{\alpha^2 S_2^2}\frac{B}{\rho_a}\sin\theta. \tag{5}$$

Integration of (5) gives

$$U^2 = U_0^2\left(\frac{x_0}{x}\right)^4 + \tfrac{2}{3}C\frac{1}{x}[1-(x_0/x)^3], \tag{6}$$

where U_0 is an initial velocity, C is the right-hand side of equation (5) and x_0 is the distance from the virtual origin to the initial state of the thermal of volume per unit width $Q_0 = S_1 H_0 L_0$. If the cloud could be released with a shape corresponding to the developed state and with the appropriate vorticity, then x_0 would just be the distance from the virtual origin to the position of release. In practice this is impossible to achieve, which means that the initial similarity state of the thermal is situated downstream of the release gate.

When the cloud is released with an initial velocity smaller than its maximum velocity it will go through an accelerating phase just after release and then decelerate. An acceleration phase is observed when

$$x < x_0\left(4 - \frac{6x_0U_0^2}{C}\right)^{\frac{1}{3}}$$

and

$$U_0 < \left(\frac{2C}{3x_0}\right)^{\frac{1}{2}}.$$

When $U_0 = 0$,

$$U \simeq \left(\frac{2C}{x_0}\right)^{\frac{1}{2}}\frac{x_0}{x}\left(\frac{x}{x_0}-1\right)^{\frac{1}{2}} \quad \text{for} \quad 1 \leqslant \frac{x}{x_0} < 4^{\frac{1}{3}}.$$

On the other hand when

$$x > x_0\left(4 - 6\frac{x_0U_0^2}{C}\right)^{\frac{1}{3}}$$

the thermal is in its decelerating phase.

For large values of x such that $(x_0/x)^3 \ll 1$ and taking $U_0 = 0$, equation (6) gives

$$U = K(g_0' Q_0 \sin\theta)^{\frac{1}{2}}x^{-\frac{1}{2}} \tag{7}$$

with

$$K = \frac{1}{S_2\alpha}\left(\frac{8S_1}{3(1+k_v)}\right)^{\frac{1}{2}}, \tag{8}$$

which is a function of θ since α, S_1/S_2 and k_v vary with θ. The coefficient K can be calculated from shape factor and growth rate measurements and compared with direct velocity measurements.

† The theory would also be valid for laminar thermals with α taking on a lower value. Assuming that the thermal is either laminar or turbulent throughout the motion implies that α is independent of x.

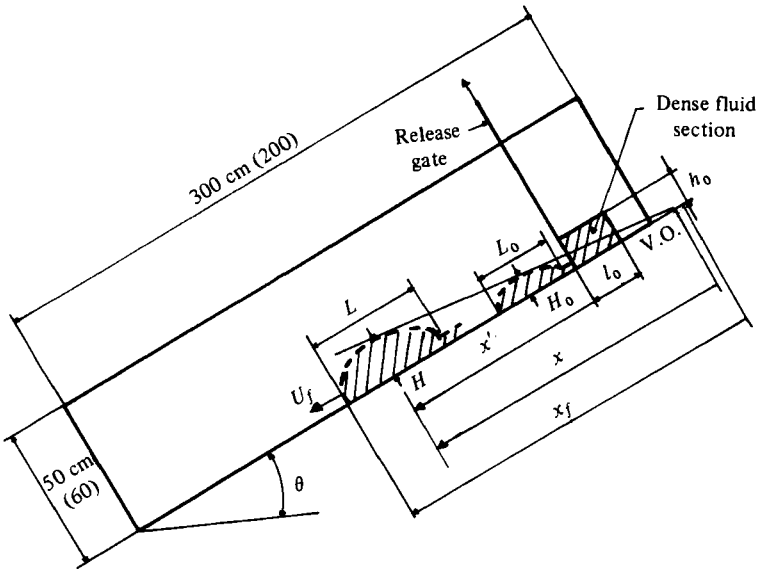

FIGURE 1. Sketch of the experimental set-ups. V.O. stands for virtual origin. Note that the virtual origins for x and x_f do not coincide.

Development in time

The development in time is also of some interest. Taking as characteristic time and velocity scales

$$t_c = \frac{Q_0^{\frac{1}{3}}[4S_1^{\frac{1}{2}}(1+k_v)]^{\frac{1}{3}}}{(S_2\alpha g_0' \sin\theta)^{\frac{1}{2}}}, \quad U_c = \frac{4S_1(\frac{1}{2}Q_0)^{\frac{1}{2}}}{S_2\alpha t_c},$$

equations (1) and (2) can be easily integrated to give

$$U^* = \frac{t^* + U_0^*}{H^*L^*}, \tag{9}$$

and

$$(H^*L^*)^{\frac{3}{2}} = 3t^{*2} + 6U_0^*t^* + 1, \tag{10}$$

where the stars indicate non-dimensional quantities and $H^*L^* = HLS_1/Q_0$. For short times $t < t_c$ such that $((H^*L^*)^{\frac{1}{2}} - 1) \ll 1$ equations (9) and (10) give (taking $U_0 = 0$)

$$(H^*L^*)^{\frac{1}{2}} - 1 \approx t^{*2}, \quad U^* \approx t^*$$

and when $t \gg t_c$ $\quad (H^*L^*)^{\frac{1}{2}} \approx 3^{\frac{1}{3}}t^{*\frac{2}{3}}, \quad U^* \approx 3^{-\frac{2}{3}}t^{*-\frac{1}{3}}.$

The circulation K^* is given by $U^*(H^*L^*)^{\frac{1}{2}}$ which is

$$K^* = t^{*\frac{1}{3}}/(3 + 1/t^{*2})^{\frac{1}{3}},$$

showing that K^* increases with time. For $t \gg t_c$, $K^* \approx t^{*\frac{1}{3}}$.

3. Experimental set-up and procedures

The experiments were carried out in two different water tanks made of Perspex, a sketch of which is shown in figure 1. Both tanks were completely closed and were 30 cm wide and one was 50 cm deep and 300 cm long and could be set at any angle

from 0 to 40°, and the other 60 cm deep and 200 cm long inclinable from 45° to 90°. In each of these tanks a release gate spanning the width of the tank was positioned near one end of the tank. Behind this gate the dense fluid was introduced into the space $h_0 \times l_0 \times 30$ cm (see figure 1). Pressure head control tubes allowed the adjustment of the heads before release. Usually a common-salt solution was used as dense fluid but some runs were made with sand suspensions. The initial volumes per unit width of the dense fluid studied were in both tanks 8 cm deep (h_0) and 10 cm long (l_0), giving $Q_0 = 80\,\text{cm}^2$. Volumes of 11·5 cm depth and 20 cm length were also released in the low angle tank and 10 cm depth and 20 cm length in the vertical tank.

For the experiment the tank was positioned and then filled with fresh water. The dense fluid was slowly introduced behind the release gate in the space $h_0 \times l_0 \times 30$ cm, displacing the fresh water.† After adjustment of the pressure heads the gate was suddenly withdrawn and the dense fluid started to flow down the slope.

Flow visualization methods were used to obtain the size and geometry of the flow, the velocity of the advancing front and the internal structure. Usually the dense fluid was dyed with rhodamine and measurements were made from photographs taken at regular time intervals. Slit lighting and aluminium particles in suspension gave some indication of the internal vortex structure. The camera was in this case displaced with the front velocity.

From the photographs it is relatively easy to define the front position, whereas the bulgy nature of the contour (see for instance figures 2*b* and 2*d*) and the existence of a wake made the determination of the height and, in particular, the length of the buoyant cloud at low slope angles somewhat subjective. Generally the contour used for defining the height and length was a somewhat smoothed contour; that is to say, localized small protrusions were averaged out. For $\theta = 90°$ the interface after withdrawal of the barrier is unstable over the whole depth and there is no preferential position where motion should start. The resulting irregular initial conditions influence the initial development of the thermal. In order to reduce this difficulty the experiments were performed with 89°, which favoured flow commencement near the wall.

4. Experimental results

4.1. *Qualitative observations*

A two-dimensional thermal on inclined boundaries is similar in structure to the head of an inclined starting plume studied by Hopfinger & Tochon-Danguy (1977) and Britter & Linden (1980). Both can be approximated by a half-ellipse and as will be seen in §4.2 the height-to-length ratio is practically the same. Figure 2 shows photographs of inclined thermals for slope angles $\theta = 5$, 25, 45, 60, 75 and 90°. The decrease of the length-to-height ratio L/H with slope angle is clearly seen from this figure. Similarity theory assumes that this ratio is a constant for a given slope angle. Experimentally it is observed, however, that this ratio initially varies somewhat with distance; increasing or decreasing depending on the geometry of the volume released and on the slope angle. For instance, for the volume $l_0 \times h_0 = 10 \times 8$ cm the ratio L/H increases for slope angles less than about 20° and decreases slightly for angles above

† When a sand suspension was used the suspension was introduced before filling the tank with fresh water. To reduce sedimentation the suspension was agitated a short time before release.

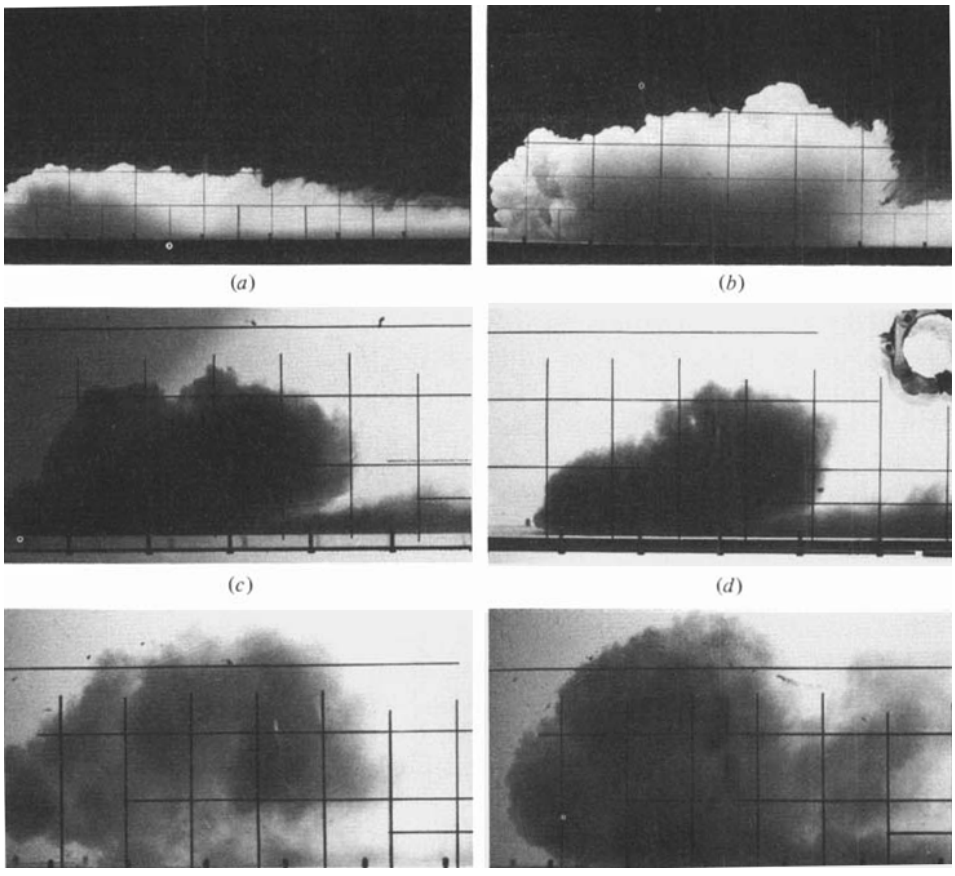

FIGURE 2. The shape of thermals on slopes 5°, 25°, 45°, 75° and 90°. The thermals move from right to left.

about 45°. For a higher aspect ratio of the released volume ($20 \times 11{\cdot}5$ cm) the ratio L/H is more nearly constant at lower angles than 20°, but decreases slightly for larger values of the slope angle. The values of length-to-height ratios which will be discussed in §4.2 are average values of the fully developed state, generally taken at $x \geqslant 10h_0$. For the same conditions of release the detailed internal flow structure of the thermal may differ from one run to another. For example, the big eddy situated at the rear of the thermal in figure 2*d* may in another run occur closer to the front. This is illustrated in figure 3, which shows a vertical slice of a thermal, on a slope of 20°, containing aluminium particles as tracers. The camera was moving with the velocity of the front. Figure 3(*a*) indicates a structure similar to that of figure 2(*d*), whereas figure 3(*b*) shows two big eddies of equal size. In spite of this variability in the detailed flow structure and the effect of the geometry of the volume released on the initial development of the length, similarity theory gives, as will be seen, a reasonably good description of the experiments.

Except at very small slope angles the boundary has little or no effect on the flow apart from it producing an overhang of the foremost front (nose). On a horizontal

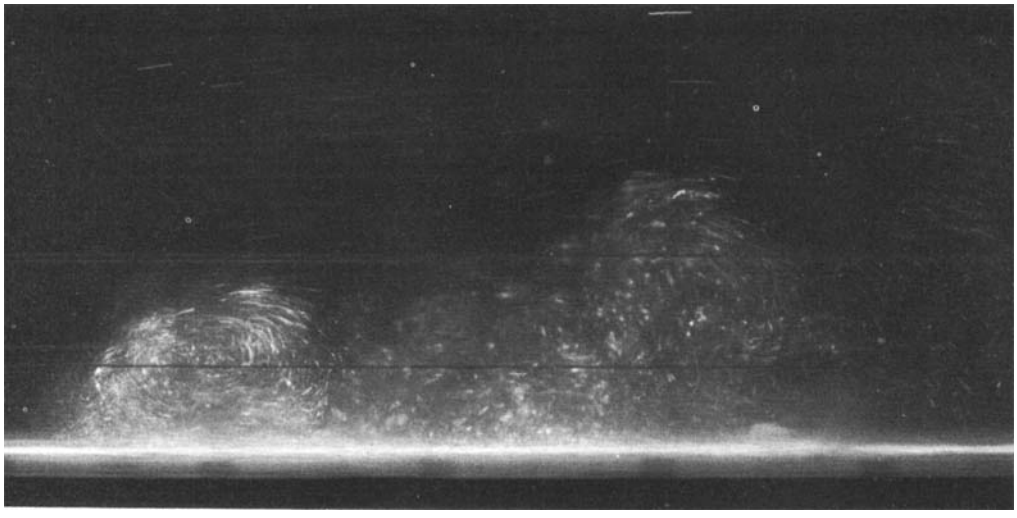

(*a*)

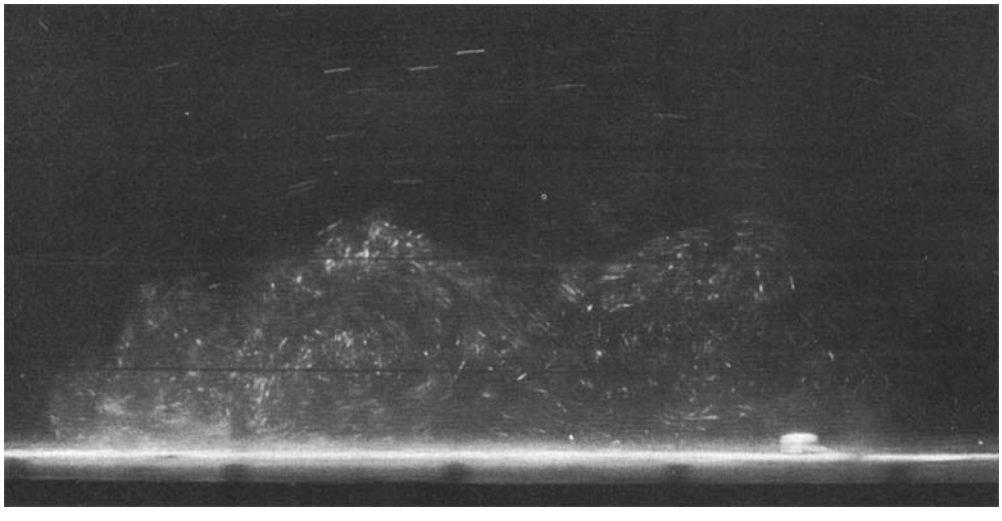

(*b*)

FIGURE 3. Internal structure of an inclined thermal moving down a slope of 20°, showing two dominant vortex centres of dissimilar sizes in (*a*) and equal size in (*b*). Conditions in (*a*) and (*b*) are otherwise identical.

boundary this overhang is well defined (Simpson 1972), whereas on inclined boundaries it varies somewhat from one cloud to another and also with distance in an inconsistent way. In the mean the nose is, however, further away from the wall at high slope angles than at low angles.

In the theoretical treatment it was also assumed that no buoyancy is lost to the wake of the thermal. However, from figure 2 it is seen that some dense fluid remains in the wake and the results indicate that for an initial volume of high aspect ratio there is a tendency for more fluid to remain in the wake (see discussion below).

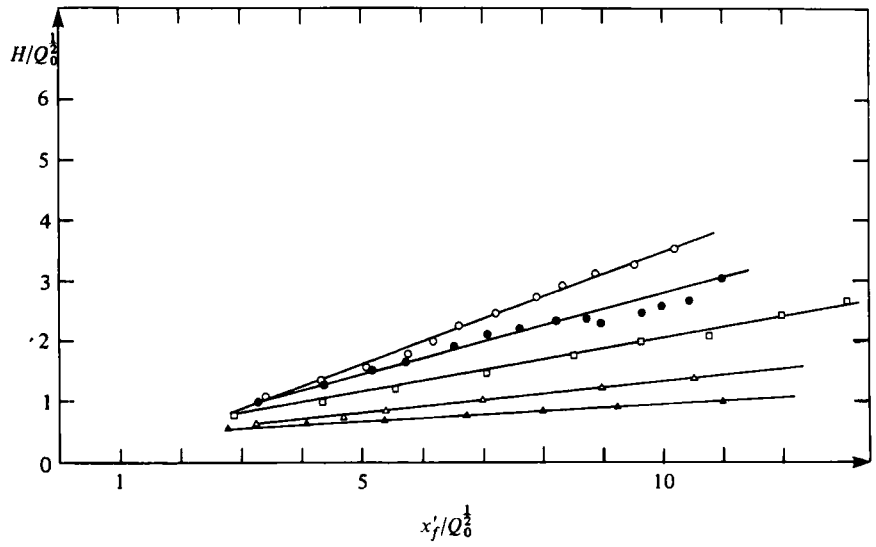

FIGURE 4. Height of the thermal as a function of distance from the gate to the front, normalized by $Q_0^{\frac{1}{2}}$. Q_0 is initial volume per unit width. ▲, 5°; △, 20°; □, 45°; ●, 75°; ○, 90°.

4.2. *Quantitative results*

In the theory the variables x and U refer respectively to the position of the mass centre measured from the virtual origin and to the mass-centre velocity. Experimentally we have direct access to the front velocity U_f and the position of the front x_f. It is for this reason that for thermals it is usual to define the rate of growth by radius, in our case the height, divided by distance to the front rather than by the half-angle of spread defined by radius divided by distance to the mass centre. Assuming a symmetric shape for the thermal, the transformations are simply

$$\left.\begin{aligned} x = x_f - \tfrac{1}{2}L \qquad &= x_f\left(1-\frac{1}{2k}\frac{dH}{dx_f}\right), \\ U = U_f\left(1-\frac{1}{2}\frac{dL}{dx_f}\right) &= U_f\left(1-\frac{1}{2k}\frac{dH}{dx_f}\right). \end{aligned}\right\} \tag{11}$$

Equations (3) and (4) remain valid when x is replaced by x_f and α by

$$\alpha_f = (1-(1/2k)\,dL/dx_f).$$

The same is true for equation (7) with K replaced by $K_f = K/(1-(1/2k)\,dH/dx_f)^{\frac{3}{2}}$. Thus only the numerical values of the coefficients change when the variables refer to the front rather than to the mass centre.

A total of 42 runs were analysed. In figure 4 the increase in height, normalized by the square root of initial volume per unit width, is shown with distance from the release gate. Figure 4 indicates that for all angles $\gtrsim 5°$ the height is a linear function of distance, in agreement with equation (3). According to the similarity assumptions the length should also grow linearly with distance and this is shown in figure 5. The length is, however, less well defined and this results in increased experimental scatter. As was pointed out in §4.1, when the length-to-height ratio just after release of the dense fluid does not correspond to the similarity state, the length initially increases

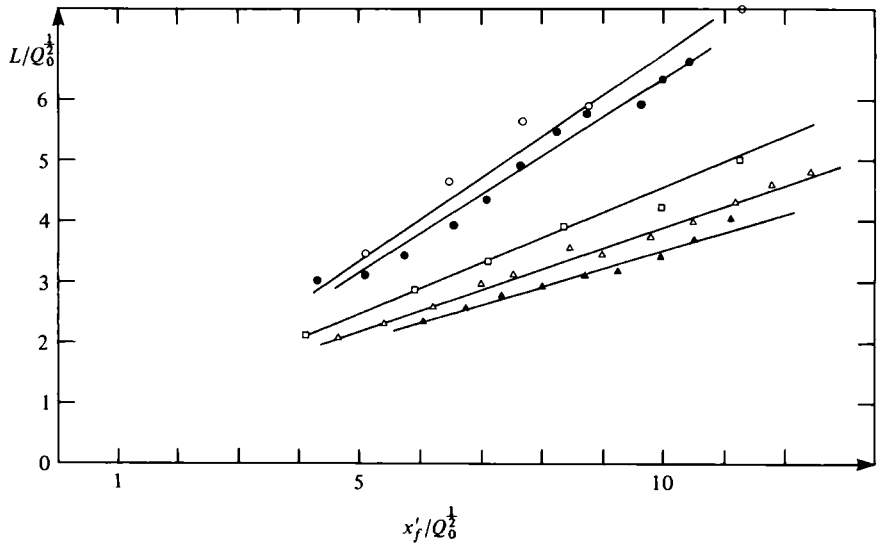

FIGURE 5. Length of the thermal as a function of distance to the front, normalized by $Q_0^{\frac{1}{5}}$. The symbols refer to the same conditions as in figure 4.

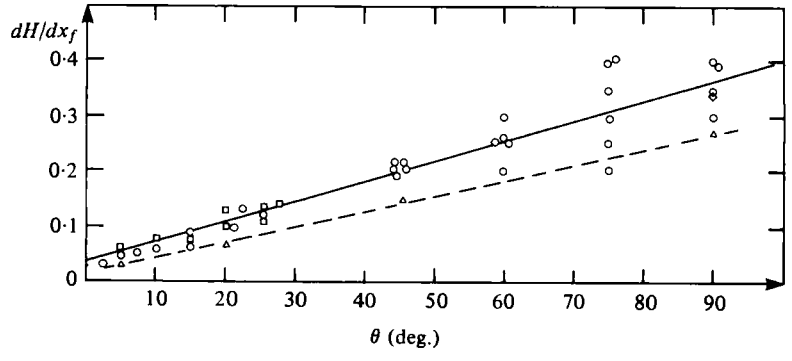

FIGURE 6. Growth rate in height as a function of slope angle θ. The symbols □ refer to the sand suspension thermal; △ and - - - - indicate the growth of a gravity current head (Britter & Linden 1980); ◇, value of line thermal of Tsang (1971); —— corresponds to $3{\cdot}6 \times 10^{-3}\theta + 0{\cdot}04$.

more or less rapidly than expected from similarity laws. This leads, at low slope angles, to some difference in virtual origins when these are determined either from length or height measurements. For larger slope angles the adjustment to a similarity state is more rapid and the two virtual origins coincide within experimental error. In the transformation equations (11) a common virtual origin is chosen and is determined by the upstream extrapolation of the thermal height to zero.

The rate of growth in height dH/dx_f as a function of a slope angle is shown in figure 6 for the range $2{\cdot}5° \leqslant \theta \leqslant 90°$. The line fitted through the data points, given by $dH/dx_f = 3{\cdot}6 \times 10^{-3}\theta + 0{\cdot}04$,† does not intercept the ordinate at zero, a behaviour also found for steady plumes (Ellison & Turner 1959). Below 5° the growth rate falls

† Linear regression indicates that the straight line fitted through the data points in figure 6 has a correlation coefficient higher than 0·9 which is a 'highly significant' value considering the large number of data points. This also holds for figure 7.

θ	k	S_1	S_2†	$\frac{1}{2}\frac{S_2}{S_1}k^{\frac{1}{2}}$	dH/dx_f	α_f	α§	dL/dx_f	$K_f \sin^{\frac{1}{2}}\theta$
0°	0·17‡	0·8	2·83	0·73	0	—	—	—	—
5°	0·20	0·85	2·68	0·70	0·055	0·078	0·081	0·30	1·93
10°	0·28	0·8	2·41	0·79	0·07	0·088	0·10	0·32	2·45
15°	0·33	0·8	2·31	0·82	0·08	0·10	0·113	0·35	2·66
20°	0·34	0·83	2·29	0·80	0·11	0·136	0·162	0·36	2·35
25°	0·37	0·83	2·27	0·83	0·12	0·144	0·172	0·40	2·45
40°	0·43	0·86	2·20	0·84	0·19	0·24	0·308	0·48	2·00
60°	0·45	0·83	2·21	0·89	0·24	0·28	0·382	0·54	1·90
75°	0·5	0·83	2·19	0·94	0·29	0·32	0·450	0·6	1·75
90°	0·53	0·86	2·20	0·93	0·36	0·39	0·59	0·66	1·55

† S_2 was calculated from $S_2 = (\pi/2^{\frac{3}{2}})\,(4k^2+1)^{\frac{1}{2}}/k^{\frac{1}{2}}$.

‡ The length is determined by tracing an equivalent ellipse through the head of the gravity current.

§ Calculated from $\alpha = \alpha_f/(1-(1/2k)\,dH/dx_f)$.

TABLE 1. Characteristic coefficients for the thermal at slope angles ranging from 0 to 90°.

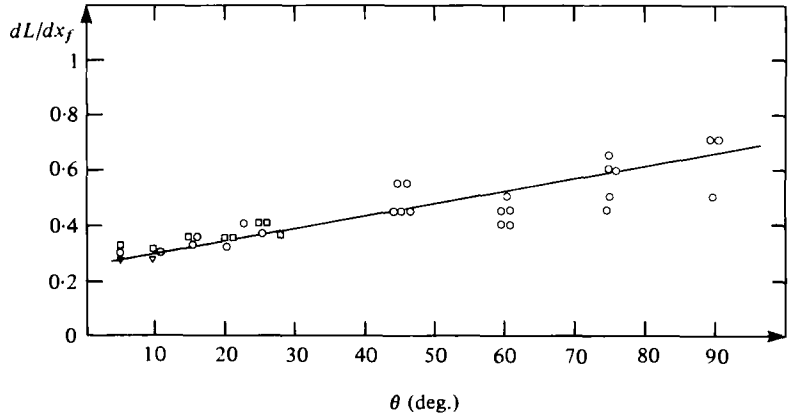

FIGURE 7. Growth rate in length as a function of slope angle θ. □, sand suspension thermal; ▽, $dH/dx_f \times (L/H)$; ——, $4{\cdot}4\times10^{-3}\theta+0{\cdot}26$.

off more rapidly and is close to zero at 0°, the precise value depending on the ratio of cloud height to depth of ambient fluid. Figure 6 indicates that for $\theta \gtrsim 5°$ dH/dx_f is a linear function of θ. In table 1 the values for the shape factor coefficients, the height-to-length ratio k and the values of α and α_f are given. When plotting α_f or α as a function of slope angle it is noticed that α_f and α are, within experimental error, also linear functions of θ.

Figure 7 shows the rate of increase in length as a function of θ. A straight line given by $dL/dx_f = 4{\cdot}4\times10^{-3}\theta+0{\cdot}26$ is a good fit to the data in the range $5° \lesssim \theta \leqslant 90°$. The ratio $(dL/dx_f)/(dH/dx_f)$ presented in figure 8 increases with decreasing slope angle, and because of the lack of a strict similarity development at low slope angle this ratio exceeds the length-to-height ratio, which is also given in figure 8. It is interesting to note that the length-to-height ratio for the head of an inclined starting plume (Britter & Linden 1980) shows a variation with θ very much like the inclined thermal. The

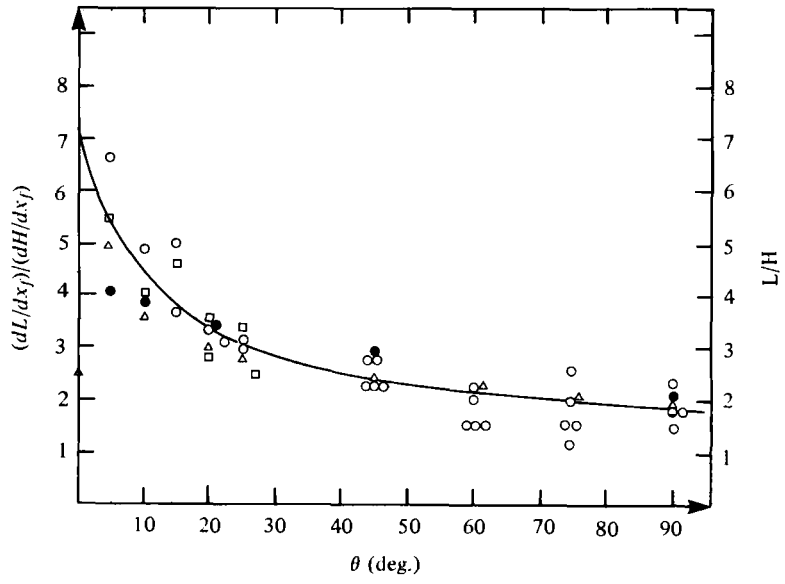

FIGURE 8. Ratio of spatial growth rates in length and height indicated by ○ and □ and of length-to-height ratio, indicated by △, as a function of slope angle θ. ●, length-to-height ratio for a gravity current head (Britter & Linden 1980). ——, $(4{\cdot}4\times10^{-3}\theta+0{\cdot}26)/(3{\cdot}6\times10^{-3}\theta+0{\cdot}04)$.

spatial growth of the head of the starting plume is, however, less than that of the thermal (figure 6).

In all the experiments the dense fluid was released without an initial velocity, so that the cloud went through an acceleration phase just after release and then decelerated. This is clearly seen from figure 9, where the normalized mass centre velocity for a slope angle of 10° is plotted as a function of distance to the mass centre normalized by x_0, which is the distance from the initial similarity state to the virtual origin. The latter can be obtained by extrapolating H as a function of x' (distance from the release gate to the mass centre, see figure 1) upstream of the gate to $H = 0$. The value of x_0 used in figure 9 was, however, determined from $x_0 = h_0/(2dH/dx)$, which was a fairly good representation of x_0. When the gate is opened the dense fluid emerges with a height $\frac{1}{2}h_0$, but, because it emerges without vorticity and an aspect ratio generally different from that of the similarity state, it moves a short distance downstream (of order h_0) before a similarity state is established. This is the reason for the downstream displacement of the maximum of the experimental curve with respect to the theoretical one. By shifting the origin by about h_0 the locations of the two maxima could be made to coincide. The distinct jump in the experimental points at $x/x_0 = 2$ has no physical significance and is merely due to the error associated with finite-differencing the data.

Figure 9 also indicates that the observed velocity is about 10–20% higher than the velocity predicted by equation (6). As is seen from table 2, this is generally the case for slope angles $\theta \leqslant 45°$ and $l_0/h_0 \simeq 1$. Taking the virtual mass coefficient equal to zero at these slope angles would give good agreement of theory with experiments. Table 2 also shows that the time of acceleration decreases rapidly when θ increases.

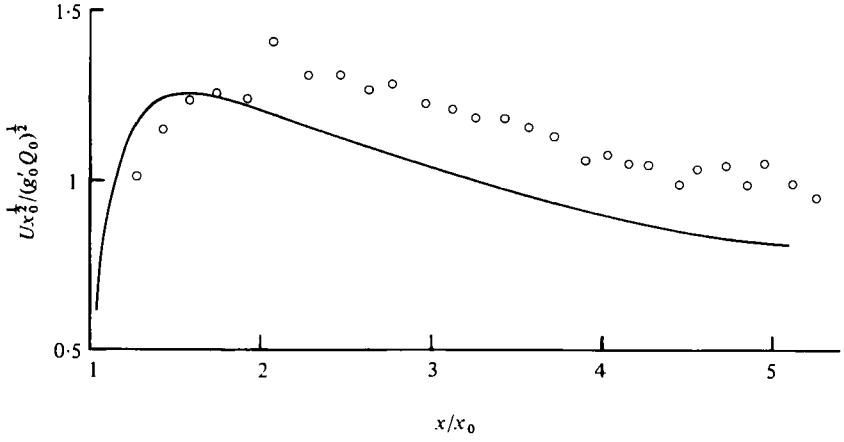

FIGURE 9. Mass centre velocity on 10° slope, normalized by $(g_0' Q_0/x_0)^{\frac{1}{3}}$, as a function of distance to the mass centre measured from the virtual origin and normalized by $x_0 = 45$ cm. ——, equation (6); ○, experimental points. x_0 is the distance from the virtual origin to the actual origin (taken as the gate of release).

θ	k_v	Q_0 (cm^2)	ρ_0/ρ_a%	t_c (s)	$U_{f\max}$ (cm s^{-1})	$U_{f\max(k_v=0)}$ (cm s^{-1})	$U_{f\max}$(exp) (cm s^{-1})
5°	0·4	80	2	10·5	6·01	—	—
10°	0·56	80	2	7·42	7·56	9·41	10
15°	0·66	80	2	6·32	8·95	11·53	10
20°	0·68	80	2	4·83	9·13	11·83	13
45°	0·86	80	2	2·55	9·88	13·4	13
			15	0·93	27·14	37·0	35
60°	0·90	80	2	2·07	10·22	14·08	13
75°	1·0	80	2	1·87	10·00	14·1	13
			15	0·68	27·51	38·78	30
90°	1·0	80	2	1·60	10·02	14·2	10
			15	0·58	27·65	54·8	32

TABLE 2. Values of characteristic acceleration time and of maximum front velocity for different slope angles.

During the decelerating state equation (7) indicates that the velocity is proportional to $x_f^{-\frac{1}{2}}$, which agrees with experiments (figure 10). The experimental scatter at large slope angles is, however, considerable. This scatter is inherent to thermals on large slopes and is a consequence of the observed intermittent outgrowths as the flow proceeds. It is nevertheless reasonable to assume the velocity coefficient K_f to be constant for a given slope angle, but figure 10 indicates that the non-dimensional velocity $U_f x_f^{\frac{1}{2}}/(g_0' Q_0)^{\frac{1}{3}} = K_f \sin^{\frac{1}{3}}\theta$ is a decreasing function of θ. This variation of $K_f \sin^{\frac{1}{3}}\theta$ with slope angle is brought out in figure 11, where $K_f \sin^{\frac{1}{3}}\theta$ is plotted as a function of slope angle. It is seen that the non-dimensional velocity reduces from a maximum of about 2·6 at 10°–20° to a value of about 1·5 at 90°. The large experimental scatter, in particular for large slope angles, is again apparent from figure 11 and is similar to the scatter in non-dimensional velocity observed for the inclined

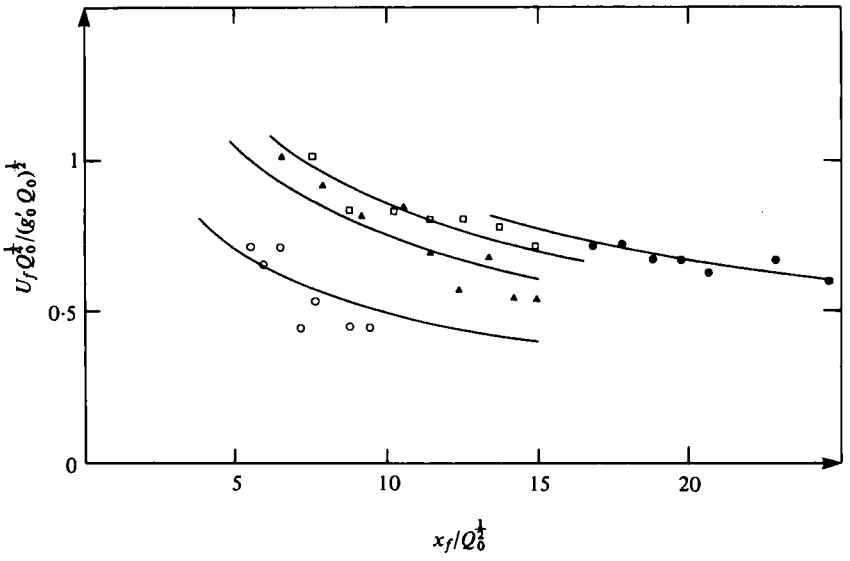

FIGURE 10. Front velocity normalized by the square root of the buoyancy released, as a function of distance to the front measured from the virtual origin. The solid lines are curves $U_f \propto x_f^{-\frac{1}{2}}$ fitted to the data points. ●, $\theta = 10°$; □, $\theta = 45°$; ▲, $\theta = 60°$; ○, $\theta = 90°$.

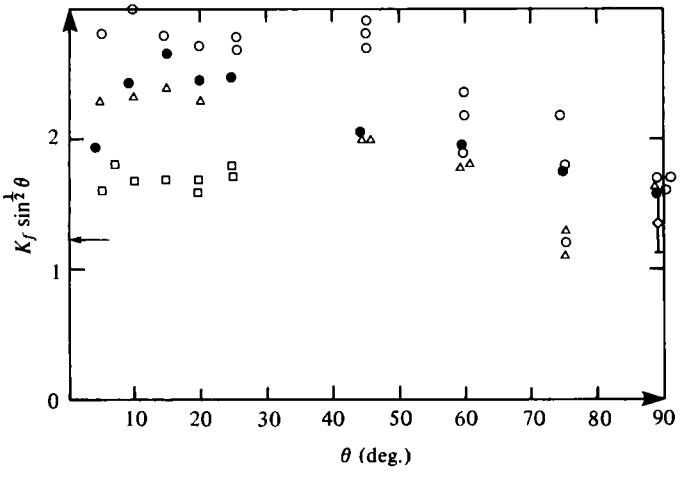

FIGURE 11. Velocity coefficient $K_f \sin^{\frac{1}{2}}\theta$ as a function of slope angle θ. ○, $Q_0 = 80$ cm²; △, $Q_0 = 230$ cm²; □, sand suspension $Q_0 = 80$ cm²; ●, calculated from equation (8) transformed to front variables using values given in table 1; ◇, Tsang's resultt for line thermals; ←, $U_f(x_f'/g_0' Q_0)^{\frac{1}{2}}$ for finite volume release on zero slope.

starting plume (Britter & Linden 1980). The non-dimensional velocity calculated from equation (7) together with (8) (transformed to front variables) and using the values given in table 1, gives a good representation of the measured front velocity.

It is seen from figure 11 that values of $K_f \sin^{\frac{1}{2}}\theta$ for the sand suspension thermals are lower than for the brine thermals. This is not surprising, since sedimentation of sand before release, and to some extent also during the motion, is inevitable and the

effective g_0' must be lower than the nominal value of g_0'. This does not, however, affect the growth rate of sediment thermals, which was found to be identical with brine thermals (figure 6). The sand used was graded to give grain sizes less than 20 μm which have a fall velocity under gravity much less than the convective velocity inside the thermal.

For low slope angles figure 11 also indicates that the velocity coefficient K_f may depend on the initial volume or more likely the aspect ratio of the released volume. For volumes $Q_0 = 80$ cm^2 of aspect ratio l_0/h_0 close to 1, the non-dimensional velocity is higher than for volumes $Q_0 = 230$ cm^2 (or 200 cm^2) of aspect ratio closer to 2. Because the dense fluid emerges from the gate with height $\frac{1}{2}h_0$, it starts off more like a starting plume when the aspect ratio l_0/h_0 is large. This flow then develops into a thermal structure as dense fluid from the layer behind the head flows into the head. However, as the layer behind the head gets thinner its velocity, because of mass loss to the head, drops below the front velocity and it eventually remains there as a wake. It is therefore quite possible that more buoyancy remains in the wake when the aspect ratio at release is large.

It is also noticed that at low slope angles the measured normalized velocity for $Q_0 = 80$ cm^2 is generally greater than the value calculated from equation (8). One explanation, as mentioned before, is that the added mass coefficient is less than $2k$ as it would be for an elliptically shaped body. Because of the large eddy structures as shown in figure 2 fluid is entrained on the back of the first eddy and also through the whole boundary, and this leads to a streamline pattern quite different from that of the flow around an elliptic solid body. At larger slope angles the flow consists of only one main eddy and in this case a virtual mass coefficient of about 1 would seem more plausible.

A more curious behaviour exhibited by figure 11 is the variation of front velocity with slope angle. The initial increase in normalized velocity as the slope angle increases from very small values, and the decrease for slope angles larger than about 15° are consequences of the different dependence of driving force and retarding mechanism (entrainment of ambient fluid) on slope angle. The dependence of driving force on slope angle is clear, but the reason for the observed linear dependence of the entrainment rate on θ is unexplained.

5. Behaviour for slopes less than 5°

As the slope is reduced below 5° the previous interpretation and analysis of the experiment becomes less applicable. For example, when the slope is horizontal, $\theta = 0°$, the dense fluid spreads, with mixing between the fluids restricted to near the leading edge. This leading edge is, of course, a gravity current head (see Britter & Simpson 1978). Thus most of the denser fluid remains unmixed in a layer of decreasing thickness. Therefore, at very small slopes, the concept of a well-mixed, identifiable, buoyant cloud is not applicable. Experiments at a slope of 2·5° indicated that the flow was to some extent similar to that at 5°. All the dense fluid appeared to be involved in the mixing, but the length of the head was poorly defined, with some mixed fluid left well behind the leading edge. It seemed, therefore, inappropriate to consider this very large and poorly defined region as being a cloud of elliptical shape.

It is noteworthy that on zero slope the front velocity, after the acceleration phase

terminated, could be represented by $U_f/(g'_0 Q_0)^{\frac{1}{3}} \propto x_f'^{-\frac{1}{3}}$. The distance to the leading edge was now measured from the gate rather than from a virtual origin. Using data from Hoult (1972), who found a similar spatial velocity dependence, the proportionality constant may be estimated as 1·23. This value is indicated in figure 11 for comparison. In the present experiments the dense fluid layer thickness was much less than the depth of the total fluid. When the dense fluid layer is an appreciable fraction of the total depth a quite different behaviour of constant U_f is observed (Huppert & Simpson 1980).

Owing to the limited size of the apparatus viscous effects became important shortly after release when the slope angle was close to zero and this prevented us reaching any more definite conclusions concerning the flow on very small slopes.

6. Conclusions

It has been shown that the 'thermal theory' can be applied to the motion of buoyant clouds moving on slopes of angles $5° \lesssim \theta \leqslant 90°$. The coefficients are now functions of slope angle θ and the basic entrainment coefficient α is multiplied by shape factor coefficients whose product is 1 when $\theta = 90°$ and $\frac{3}{4}$ when $\theta \simeq 5°$ (see table 1). The spatial growth rates in height and length of the cloud are linear functions of the slope angle and are larger than the corresponding growth rates for the head of an inclined starting plume. The length-to-height ratio of the head of an inclined starting plume can, however, be considered identical to that found for the inclined thermal. The thermal is well represented by a half-ellipse, as is apparent from the shape factor coefficient S_1 given in table 1.

When the dense fluid is released without initial velocity it goes through an acceleration phase and then decelerates. The time of acceleration is reasonably well predicted by theory, considering that the dense fluid is released without initial vorticity and that the cross-sectional area of released volume does not correspond to the developed half-elliptic shape. The acceleration time decreases by roughly a factor of 10 as the slope angle increases from 5° to 90°. The maximum front velocity normalized by $(g'_0 Q_0)^{\frac{1}{3}}$ increases weakly with slope angle (table 2) ,whereas the non-dimensional front velocity in the decelerating state $U_f/(g'_0 Q'_0/x_f)^{\frac{1}{3}}$ has a maximum of $2{\cdot}6 \pm 0{\cdot}2$ at 15° and then falls off uniformly to a value of $1{\cdot}5 \pm 0{\cdot}2$ at 90°. The thermal theory, which requires experimental values of α and k, is in good agreement with this behaviour.

The transition from a thermal structure to a gravity current, similar to that on horizontal boundaries, takes place at an angle less than 5°. The flow seems to merge gradually from one state to another as the slope angle is decreased below 5°. More quantitative conclusions concerning the flow along horizontal or weakly inclined boundaries await further study using an apparatus of larger dimensions to reduce viscous effects.

This research was partially supported by a grant from the Centre Technique du Génie Rural et des Eaux et Forêts. One of the authors, Dr Britter, acknowledges support from the CNRS during his stay at the Institute de Mécanique.

REFERENCES

BATCHELOR, G. K. 1967 *An Introduction to Fluid Dynamics*. Cambridge University Press.

BRITTER, R. E. & LINDEN, P. F. 1980 The motion of the front of a gravity current travelling down an incline. *J. Fluid Mech.* **99**, 531–543.

BRITTER, R. E. & SIMPSON, J. E. 1978 Experiments on the dynamics of a gravity current head. *J. Fluid Mech.* **88**, 223–240.

ELLISON, T. H. & TURNER, J. S. 1959 Turbulent entrainment in stratified flows. *J. Fluid Mech.* **6**, 432–448.

HOPFINGER, E. J. & TOCHON-DANGUY, J. C. 1977 A model study of powder-snow avalanches. *J. Glaciology* **19**, 343–356.

HOULT, D. P. 1972 Oil spreading on the sea. *Ann. Rev. Fluid Mech.* **4**, 341–368.

HUPPERT, H. E. & SIMPSON, J. E. 1980 The slumping of gravity currents. *J. Fluid Mech.* **99**, 785–799.

MORTON, B. R., TAYLOR, G. I. & TURNER, J. S. 1956 Turbulent gravitational convection from maintained and instantaneous sources. *Proc. Roy. Soc.* A **234**, 1–23.

SIMPSON, J. E. 1972 Effects of the lower boundary on the head of a gravity current. *J. Fluid Mech.* **53**, 759–768.

TOCHON-DANGUY, J. C. & HOPFINGER, E. J. 1975 Simulation of the dynamics of powder avalanches. *Proc. Grindelwald Symp., IAHS Publ.* No. 114, pp. 369–380.

TSANG, G. 1971 Laboratory study of line thermals. *Atm. Env.* **4**, 445–471.

TURNER, J. S. 1962 The 'starting plume' in neutral surroundings. *J. Fluid Mech.* **13**, 356–368.